Polyhedron 54 (2013) 260–271

Contents lists available at SciVerse ScienceDirect

Polyhedron

journal homepage: www.elsevier.com/locate/poly

Mono-, di- and trinuclear complexes of bis(terpyridine) ligand: Synthesis, crystal structures and magnetic properties

Monika Wałęsa-Chorab [a], Adam Gorczyński [a], Maciej Kubicki [a], Maria Korabik [b], Violetta Patroniak [a,*]

[a] Faculty of Chemistry, Adam Mickiewicz University, Grunwaldzka 6, 60780 Poznań, Poland
[b] Faculty of Chemistry, University of Wrocław, 14 Joliot-Curie, 50383 Wrocław, Poland

ARTICLE INFO

Article history:
Received 17 December 2012
Accepted 25 February 2013
Available online 6 March 2013

Keywords:
Cobal
Copper
Manganese
Magnetic properties
Self-assembly

ABSTRACT

Application of Stille-coupling protocol allowed for synthesis of new bis(terpyridine) ligand **L** (6′,6″-(2-phenylpyrimidine-4,6-diyl)bis(6-methyl-2,2′-bipyridine)) which comprises two tridentate N-donor subunits, designed so as to exploit the formation of supramolecular architectures of different nuclearity. Further complexation, while maintaining reaction parameters unaltered, with the following salts: $CoCl_2$ (**1**), $Co(NO_3)_2$ (**2**), $Cu(NO_3)_2$ (**3**) and $Mn(ClO_4)_2$ (**4**) led to three different classes of compounds: mono-, di- and trinuclear species, the result of self-assembly being contingent on the choice of the metal ion as well as to its corresponding counterion. Single crystal structures of $[Co(\mathbf{L})Cl_2]$ (**1**), $[Co_2(\mathbf{L})(NO_3)_4](CH_3CN)_2$ (**2**), $[Cu_2(\mathbf{L})(NO_3)_4](CH_3CN)_2$ (**3**) and $[Mn_3(\mathbf{L})_2(H_2O)_2(CH_3CN)_4](ClO_4)_6{\cdot}2H_2O$ (**4**) are presented, together with description of their magnetic behavior. Delusively simple coordination compounds were found to self-assemble into interesting supramolecular architectures in the solid state: 1D pillar-like constituent arranged in the helical manner (**1**), sheets of isostructural **2** and **3**, hydrogen bonded zig-zag shaped chains (**4**). Magnetic susceptibility measurements made the determination of both antiferromagnetic interactions and metal ions′ multiplicity possible.

1. Introduction

Concepts such as *molecular recognition* and *self-organisation* introduced by J.M. Lehn and embedded within the domain of supramolecular chemistry have granted additional attention to reversible, directional interactions, the most important being hydrogen [1] and dative bonds [2]. If one anticipates to conduct preprogrammed self-assembly, among variety of factors to consider, it is careful design of ligand that is especially important as far as formation of multicomponent structures such as grids [3–6] or helicates [7–9] is concerned. One of the most spectacular recent examples shows how a slight change in the ligands bend angle critically switches the outcome of self-assembly between $M_{24}L_{48}$ and $M_{12}L_{24}$ coordination spheres [10].

It is unwise to forget about counterions which are very often chosen so as not to disrupt favorable molecular recognition outcomes, albeit their misleadingly insignificant role is usually underrated, not to say overlooked [11]. They may be *per se* responsible for a variety of factors ranging from surfactants [12] and vessel formation [13], stability of mesogenic materials [14], morphology and size of nanocrystals [15] to finish on the structure of coordination polymers, with emphasis being put on silver [16], which is the inherent domain of crystal engineering.

Ligands bearing terpyridine and parent-like moieties have been found to be particularly appealing what is, in connection with various modes of coordination to metal ions, reflected by their utilization in numerous fields such as nanotechnology [17], catalysis [18], bioassays [19] and polymer science [2].

When it comes to cobalt and manganese ions, variety of oxidation states they may adopt – especially in the case of the latter one – makes the assumption of catalytic and magnetic properties logical and obvious in connection with rigid, multidentate, properly designed N-donor ligand. Cobalt compounds, although well known for their catalytic activities in fields such as organometallic chemistry [20] have been recently highlighted for both oxidative and reductive reactions in terms of the water splitting process [21]. When magnetic properties are under evaluation such as spin-canting [22], spin-frustration [23], spin-flop transitions [24], or metamagnetism [25] manganese(II) is the metal of choice, provided, thesis being above all supported by work of Zhao and co-workers, where Kagomé layer-based 3D Mn(II) framework showed coexistence of all four aforementioned phenomena [26].

Herein we report the synthesis of new N-heterocyclic ligand **L** (Fig. 1) bearing two tridentate, terpyridine-like moieties capable of forming transition metal complexes of various nuclearity, namely: mono- $[Co(\mathbf{L})Cl_2]$ (**1**), di- $[M_2(\mathbf{L})(NO_3)_4]$ (where M – Co(II)

* Corresponding author. Fax: +48 618291508.
E-mail address: violapat@amu.edu.pl (V. Patroniak).

0277-5387/$ - see front matter © 2013 Elsevier Ltd. All rights reserved.
http://dx.doi.org/10.1016/j.poly.2013.02.054

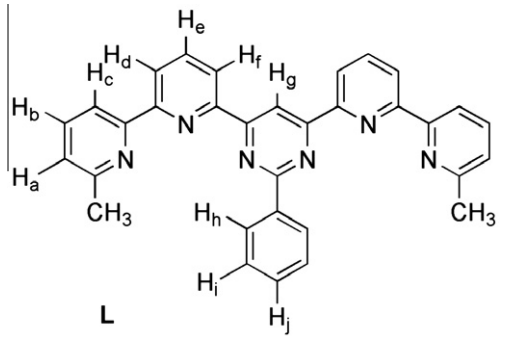

Fig. 1. Schematic representation of bis(terpyridine) ligand **L** and its labeling for ^{1}H NMR spectroscopic assignements.

– **2** or Cu(II) – **3**) and trinuclear $[Mn_3(\mathbf{L})_2(H_2O)_2(MeCN)_4](ClO_4)_6$ (**4**) species, which may be altered and controlled by the choice of the metal ion and its corresponding counterion. Complexes have been characterized in terms of crystal structure, spectroscopic and magnetic properties.

2. Experimental

2.1. General

The metal salts and reagents were used without further purification as supplied from Aldrich or Acros Organics. 2-(6-Methylpyridin-2-yl)-6-(trimethylstannyl)pyridine **A** was prepared by the substitution of 2-methyl-6-(trimethylstannyl)pyridine with 2,6-dibromopyridine via Stille coupling that resulted in acquisition of 6-bromo-6′-methyl-2,2′-bipyridine in 60% yield, which was consequently converted to **A** by bromium exchange quenching protocol with Sn_2Me_6 as previously reported by us [27]. 4,6-Dichloro-2-phenylpyrimidine b was synthesized according to the literature [28]. NMR spectra were run on a Varian Gemini 300 MHz spectrometer and were calibrated against the residual protonated solvent signals ($CDCl_3$: δ = 7.24) and are given in ppm. Electrospray Ionisation mass spectra for acetonitrile solutions ($\sim 10^{-4}$ M) were determined using a Waters Micromass ZQ spectrometer. Sample solutions were introduced into the mass spectrometer source with a syringe pump at a flow rate of 40 μL/min^{-1} with a capillary voltage of +3 kV and a desolvation temperature of 300 °C. The source temperature was 120 °C. The cone voltage (V_c) was set to 30 V to allow transmission of ions without fragmentation processes. Scanning was performed from m/z = 100–2000 for 6 s, and 10 scans were summed to obtain the final spectrum. Microanalyses were obtained using a Perkin–Elmer 2400 CHN microanalyzer. Fast Atom Bombardment spectra were determined by FAB+ using a ZAB-HF VG apparatus in an m-nitrobenzyl alcohol matrix. IR spectra were obtained with a Perkin–Elmer 580 spectrophotometer and are reported in cm^{-1}. The metal salts and reagents were used without further purification as supplied from Aldrich or Across.

Caution! Perchlorate complexes of metal ions in the presence of organic ligands are potentially explosive. Only a small amount of material should be used and handled with care.

2.1.1. 6′,6′-(2-phenylpyrimidine-4,6-diyl)bis(6-methyl-2,2′bypiridine) ***L***

To a mixture of crude 2-(6-methylpyridin-2-yl)-6-(trimethylstannyl)pyridine **A** (1.414 g, 4.25 mmol), 4,6-dichloro-2-phenylpyrimidine **B** (0.382 g, 1.70 mmol), $Pd(PPh_3)_4$ (0.246 g, 0.2 mmol) and LiCl (0.305 g, 6.61 mmol), 100 mL of degassed toluene was added gradually via syringe, constantly maintaining argon atmosphere. Reaction was stirred under reflux for 24 h at 120 °C and subsequently the solvent was removed under reduced pressure on rotary evaporator. Purification by means of chromatography on alumina with CH_2Cl_2: *n*-hexane (3:2 v:v) as an eluent yielded 0.561 g (64.1%) of white powder. mp 242–245 °C, FABMS: m/z = 493.7 (M+H$^+$, 100), IR (KBr): $\nu = \nu$(C–H)$_{ar}$ 3056, 3002; ν_{as} (CH_3) 2962; ν_s(CH_3) 2852; ν(C=C)$_{py}$ 1601, 1566, 1540, 1471; ν(C=N)$_{py}$ 1444, 1438, 1384, 1371, 1365; ρ(C–H)$_{py}$ 1087, 1072; γ(C–H)$_{py}$ 995, 826, 787, 756, 695, 643 cm^{-1}. ^{1}H NMR ($CDCl_3$, 300 MHz): δ = 9.72 (s, 1H, H_g), 8.77 (dd, 4H, J = 2.1 Hz, H_d, H_f), 8.65 (d, 2H, J = 7.8 Hz, H_c), 8.62 (d, 2H, J = 8.0 Hz, H_h), 8.05 (t, 2H, J = 7.7 Hz, H_e), 7.82 (t, 2H, J = 7.7 Hz, H_b), 7.58 (m, 3H, J = 1.8 Hz, H_i, H_j), 7.26 (d, 2H, J = 6.9 Hz, H_a), 1.65 (s, 6H, CH_3) ppm. ^{13}C NMR ($CDCl_3$, 300 MHz): δ = 164.28, 164.07, 158.00, 155.93, 155.42, 153.84, 137.95, 136.89, 130.67, 128.54, 128.39, 123.49, 122.49, 121.56, 118.26, 111.71, 24.70 ppm. *Anal.* Calc. for $C_{32}H_{24}N_6$ (492.57): C, 78.03; H, 4.91; N, 17.06. Found: C, 78.05; H, 4.87; N, 17.04%.

2.2. Synthesis of transition metal ion complexes: general procedure

Complexes have been synthesized in identical manner *i.e.* by maintaining the same conditions to exclude other factors that could affect the self-assembly phenomena than metal ion and its corresponding counterion.

To the solution of ligand **L** (20.7 mg, 42.07 μmol) previously dissolved in 10 mL of CH_2Cl_2/MeCN (9:1 v:v) mixture, appropriate amount of metal salt (84.14 μmol) was added, what resulted in the change in color. After 48 h of stirring in ambient conditions solvents were removed under reduced pressure on rotary evaporator, the residue was consecutively redissolved in minute quantity of acetonitrile that afforded clear solution and precipitated by gradual addition of diethyl ether. Colored complex was filtered, washed well with Et_2O and air dried.

2.2.1. [Co(***L***)Cl_2] ***1***

Green solid was isolated with 68% yield. Crystals suitable for structure determination were grown by vapor diffusion of diisopropyl ether into an acetonitrile solution of the complex at lowered temperature. ESI-MS: m/z (%) = 586 (10) [Co(**L**)Cl]$^+$, 515 (20) [Na(**L**)]$^+$, 284 (10) [Co(**L**)(H_2O)]$^{2+}$. IR (KBr): $\nu = \nu$(C–H)$_{ar}$ 3064; ν_{as} (CH_3) 2970; ν_s(CH_3) 2924; ν(C=C) 1598, 1590, 1569, 1535, 1483, 1470; ν(C=N) 1447, 1427, 1387, 1357, 1295, 1251; δ(CH_3) 1325; ρ(C–H) 1183, 1172, 1075, 1028; γ(C–H) 1012, 920, 895, 834, 810, 798, 696, 657 cm^{-1}. *Anal.* Calc. for $[Co(C_{32}H_{24}N_6)Cl_2]$ (622.41): C, 61.75; H, 3.89; N, 13.50. Found: C, 61.74; H, 3.93; N, 13.52%.

2.2.2. [Co_2(***L***)$(NO_3)_4$]$(CH_3CN)_2$ ***2***

Yellow solid was isolated with 65% yield. Crystals suitable for structure determination were grown by vapor diffusion of toluene into an acetonitrile solution of the complex at lowered temperature. ESI-MS: m/z (%) = 881 (5) $[Co_2(\mathbf{L})(NO_3)_3(CH_3CN)_2]^+$, 796 (10) $[Co_2(\mathbf{L})(NO_3)_3]^+$, 515 (20) [Na(**L**)]$^+$, 368 (10) $[Co_2(\mathbf{L})(NO_3)_2]^{2+}$, 311 (25) $[Co(\mathbf{L})(H_2O)_4]^{2+}$, 224 (5) $[Co_2(\mathbf{L})(NO_3)]^{3+}$. IR (KBr): $\nu = \nu$(C–H)$_{ar}$ 3093; ν_{as}(CH_3) 2978; ν_s(CH_3) 2930; ν(C=C) 1602, 1572, 1537, 1511, 1485, 1473; ν(C=N) 1384, 1362, 1300, 1250; ν_{as}(NO_2) 1445, ν_s(NO_2) 1297; δ(CH_3) 1325; ρ(C–H) 1184, 1143, 1076, 1028; γ(C–H) 1011, 922, 835, 811, 796, 768, 699, 659 cm^{-1}. *Anal.* Calc. for $[Co_2(C_{32}H_{24}N_6)(NO_3)_4]$ (858.02): C, 44.77; H, 2.82; N, 16.32. Found: C, 44.83; H, 2.78; N, 16.35%.

2.2.3. [Cu_2(***L***)$(NO_3)_4$]$(CH_3CN)_2$ ***3***

Green complex was isolated with 68% yield. Single crystal suitable for XRD analysis was found via vapor diffusion of diethyl ether to the acetonitrile solution of the complex at lowered temperature. ESI-MS: m/z (%) = 804 (10) $[Cu_2(\mathbf{L})(NO_3)_3]^+$, 617 (20) [Cu(**L**)$(NO_3)$]$^+$, 493 (50) [**L**+H]$^+$, 278 (50) [Cu(**L**)]$^{2+}$. IR (KBr): $\nu = \nu$(C–H)$_{ar}$ 3086;

$\nu_s(CH_3)$ 2933; ν(C=C) 1607, 1575, 1541, 1469, 1466; ν(C=N) 1418, 1384, 1251; $\nu(NO_3^-)$ 1433, 1289; ρ(C–H) 1187, 1141, 1046, 1015; γ(C–H) 920, 885, 833, 811, 796, 767, 703, 664, 624 cm^{-1}. *Anal.* Calc. for $[Cu_2(C_{32}H_{24}N_6)(NO_3)_4]$ (867.68): C, 44.30; H, 2.79; N, 16.14. Found: C, 44.33; H, 2.82; N, 16.15%.

2.2.4. $[Mn_3(\mathbf{L})_2(H_2O)_2(CH_3CN)_4](ClO_4)_6{\cdot}2H_2O$ **4**

Yellow solid was isolated with 69% field. Single crystal suitable for XRD analysis was acquired via vapor diffusion of *tert*-butylmethyl ether to the acetonitrile solution of the complex at lowered temperature. ESI-MS: *m/z* (%) = 646 (5) $[Mn(\mathbf{L})(ClO_4)]^+$, 523 (10) $[Mn_3(\mathbf{L})_2(ClO_4)_3(CH_3CN)_3]^{3+}$, 520 (10) $[Mn(\mathbf{L})_2]^{2+}$, 515 (25) $[Na(\mathbf{L})]^+$, 495 (10) $[Mn_3(\mathbf{L})_2(ClO_4)_3(CH_3CN)]^{3+}$, 481 (5) $[Mn_3(\mathbf{L})_2(ClO_4)_3]^{3+}$, 400 (10) $[Mn_2(\mathbf{L})(ClO_4)_2]^{2+}$, 356 (5) $[Mn_3(\mathbf{L})_2(ClO_4)_2(CH_3CN)_2]^{4+}$, 273 (10) $[Mn(\mathbf{L})]^{2+}$, 282 (10) $[Mn(\mathbf{L})(H_2O)]^{2+}$, 211 (5) $[Mn_3(\mathbf{L})_2(CH_3CN)_3]^{6+}$, 191 (10) $[Mn_3(\mathbf{L})_2]^{6+}$. IR (KBr): $\nu = \nu(C–H)_{ar}$ 3107; $\nu_{as}(CH_3)$ 2971; $\nu_s(CH_3)$ 2930; ν(C=C) 1600, 1572, 1538, 1486, 1471; ν(C=N) 1396, 1385, 1360, 1292, 1247; $\delta(CH_3)$ 1325; ρ(C–H) 1183, 1143, 1130, 1020; ν_{as}(Cl–O) 1088; δ_{as}(O–Cl–O) 626; γ(C–H) 1019, 923, 827, 792, 772, 704, 659 cm^{-1}. *Anal.* Calc. for $[Mn_3(C_{32}H_{24}N_6)_2(H_2O)_2(CH_3CN)_4](ClO_4)_6{\cdot}2H_2O$ (1982.93): C, 43.61; H, 3.46; N, 11.30. Found: C, 43.70; H, 3.40; N, 11.35%.

2.3. Crystallographic studies

Diffraction data were collected at room temperature by the ω-scan technique, for **1** on a SuperNova diffractometer with mirror-monochromatized Cu K_α radiation (λ = 1.54178 Å) and for **2**–**4** on an Xcalibur diffractometer (Eos detector) with graphite-monochromatized Mo K_α radiation (λ = 0.71073 Å). The data were corrected for Lorentz-polarization and absorption effects [29]. Accurate unit-cell parameters were determined by a least-squares fit of 2700 (**1**), 2377 (**2**), 8175 (**3**) and 3886 (**4**) reflections of highest intensity, chosen from the whole experiment. The structures were solved with SIR92 [30] and refined with the full-matrix least-squares procedure on F^2 by SHELXL97 [31]. Scattering factors incorporated in SHELXL97 were used. All non-hydrogen atoms were refined anisotropically, hydrogen atoms were placed in the calculated positions, and refined as 'riding model' with the isotropic displacement parameters set at 1.2 (1.5 for methyl groups) times the U_{eq} value for appropriate non-hydrogen atom. Relevant crystal data are listed in Table 1, together with refinement details. The crystals of **1** decompose during the data collection and therefore the dataset is incomplete; also in **1** there are huge voids in the crystal structure, apparently without any interpretable electron density. In the structure of **2** and **3**, two molecules of solvent – acetonitrile fill the voids in the asymmetric part of the crystal structure. In **4** some components of the structure (the cation and two perchlorate anions) occupy the special positions of the space group Pccn, they have C_2 internal symmetry. In this structure the residual electron density was interpreted as the water molecule, weakly bound to the rest of the structure. The positions of hydrogen atoms from this water molecule have not been found.

2.4. Magnetic measurement studies

Magnetization measurements in the temperature range of 1.8–300 K were carried out on powdered samples of complexes, at the magnetic field 0.5 T, using a Quantum Design SQUID Magnetometer (type MPMS-XL5). Polycrystalline sample for magnetic measurements was obtained from pure crystals. Corrections for diamagnetism of the constituting atoms were calculated using Pascal's constants [32,33], the value of 60×10^{-6} cm^3 mol^{-1} being used as the temperature-independent paramagnetism of copper(II) ion. The effective magnetic moments were calculated from the expression:

$$\mu_{eff} = 2.83\sqrt{\chi_m^{corr} \cdot T}(B.M.) \quad (1)$$

The best exchange parameters were obtained by fitting with a good agreement factor *R* defined as follows:

$$R = \sum_{i=1}^{n} \frac{(\chi_i^{exp}T - \chi_i^{calc}T)^2}{(\chi_i^{exp}T)^2} \quad (2)$$

3. Results and discussion

We have extensively studied systems that could be applied to variety of dative-bonded supramolecular architectures, deriving from polypyridine ligands that are capable of forming complexes in bis(bidentate) $(N_2)_2$ manner, $C_{22}H_{18}N_4$ (4,6-Bis(6-methylpyridin-2-yl)-2-phenylpyrimidine) for instance [34]. Further experience has been gained, owing to studies on ligands bearing two tridentate metal ion 'pockets', as exemplified on 6,6′-(pyrimidine-4,6-diyl)bis(N,N-diethylpicolinamide) ligand, with N_2O(carbonyl) binding subunits [35,36,9]. Noted research was the starting point to synthesize ligand **L**, where meridional donor moieties would contain exclusively nitrogen donor atoms – by expansion of bis(bidentate) $(N_2)_2$ system through addition of pyridine units, thus forming $(N_3)_2$ structural arrangement. Similar bis(terpyridine) systems can be found in the literature, nevertheless investigation upon their self-assembling capacities was mainly restrained to the formation of grid-type architectures [3,4,37].

Our previous attempts to synthesize bis(terpyridine) ligand **L** ended with monosubstitution of chlorine in 4,6-dichloro-2-phenylpyrimidine and formation of $C_{21}H_{15}ClN_4$ (6-(6-chloro-2-phenylpyrimidin-4-yl)-6′-methyl-2,2′-bipyridine). The latter molecule was further complexated with $CoCl_2$ to afford mononuclear compound as proved by single crystal X-ray analysis and DFT geometry optimization [38]. Interestingly, there is a striking resemblance between mononuclear cobalt(II) chloride complexes of mono(terpyridine) ligand $C_{21}H_{15}ClN_4$ and bis(terpyridine) ligand **L** (**1**) (*cf.* crystal structures section) in terms of geometrical surrounding what, based on calculations performed for the former one, allows us to assume that Co(II) ion exists in its quadruplet state. This has been further corroborated by magnetic susceptibility measurements (*cf.* magnetic properties). The difference in bulkiness of methyl and phenyl substituents together with distorted trigonal bypiramid geometry Co(II) ion exhibits is characteristic for catalytically active species, particularly in terms of asymmetric catalysis, thus such determination is especially important [39].

Hexadentate ligand **L** was eventually prepared by palladium catalyzed cross-coupling reaction (Fig. 2) and subsequently mixed with the following transition metal salts: $CoCl_2$ **1**, $Co(NO_3)_2$ **2**, $Cu(NO_3)_2$ **3** or $Mn(ClO_4)_2$ **4** in 1:2 (**L**: metal salt) molar ratio.

Scheme 1 shows that ligand **L** forms a variety of coordination architectures, depending on the choice of the metal ion, further aided by the presence of specific counterions.

We have very recently highlighted that bis(terpyridine) ligand **L** forms dinuclear helicate architecture with $Ag(CF_3SO_3)$ salt, what was followed by the finding that silver(I) complexes noted above exhibit unusual catalytic properties in reduction of organic pollutants upon UV–Vis irradiation [40].

Even though the complexation reactions were performed under identical conditions, different architectures were obtained in terms of nuclearity variations. From single-crystal X-ray analyses it was possible to determine 'model' coordinative tendencies of the systems under study *i.e.* nitrogen donor ligand and metal ions self-assemble to form molecules of different stoichiometries, depending on metal ion chosen and its counterion. During the course of investigation it was found that both the nuclearity and degree of coordination of the complexes are a result of an interplay

Table 1
Experimental crystal data, data collection and structure refinement details.

Compound	**1**	**2**	**3**	**4**
Formula	$C_{32}H_{24}Cl_2CoN_6$	$C_{36}H_{30}Co_2N_{12}O_{12}$	$C_{36}H_{30}Cu_2N_{12}O_{12}$	$C_{72}H_{68}Cl_6Mn_3N_{16}O_{28}$
Formula weight	622.40	940.58	949.80	1982.94
Crystal system	tetragonal	monoclinic	monoclinic	orthorhombic
Space group	$I4_1/a$	$P2_1/c$	$P2_1/c$	$Pccn$
a (Å)	33.0623(8)	11.6996(8)	11.7108(9)	23.6769(5)
b (Å)	33.0623(8)	28.4396(17)	28.468(2)	14.8424(3)
c (Å)	13.1825(4)	12.1052(8)	12.1216(9)	23.2580(4)
β (°)	90	100.917(6)	100.920(7)	90
V (Å^3)	14410.0(7)	3954.9(6)	3967.9(5)	8173.4(3)
Z	16	4	4	4
d_x(g cm^{-3})	1.15	1.58	1.59	1.61
F(000)	5104	1920	1936	4052
μ (mm^{-1})	5.31	0.92	1.15	0.75
θ Range (°)	2.67–73.80	2.75–25.00	2.75–25.00	2.81–25.00
hkl range	$-25 \leqslant h \leqslant 26$, $-40 \leqslant k \leqslant 28$, $-15 \leqslant l \leqslant 11$	$-13 \leqslant h \leqslant 13$, $-33 \leqslant k \leqslant 33$, $-14 \leqslant l \leqslant 14$	$-13 \leqslant h \leqslant 13$, $-33 \leqslant k \leqslant 33$, $-14 \leqslant l \leqslant 14$	$-28 \leqslant h \leqslant 27$, $-17 \leqslant k \leqslant 17$, $-27 \leqslant l \leqslant 27$
Reflections				
Collected	6808	37072	56927	83866
Unique (R_{int})	4393 (0.020)	6958 (0.181)	6981 (0.149)	7194 (0.039)
With [$I > 2\sigma(I)$]	2592	3183	3466	5826
Number of parameters	370	563	563	7194
Weighting scheme				
A	0.0488	0.03	0.05	0.1243
B	0	0	0	56.5492
$R(F)$ [$I > 2\sigma(I)$]c	0.034	0.080	0.063	0.096
$wR(F^2)$ [$I > 2\sigma(I)$]	0.075	0.113	0.118	0.252
$R(F)$ [all data]	0.067	0.196	0.138	0.114
$wR(F^2)$ [all data]	0.084	0.142	0.130	0.263
Goodness of fit (GOF)	0.87	0.99	0.98	1.04
Maximum/minimum $\Delta\rho$ (e Å^{-3})	0.14/−0.19	0.43/−0.43	0.68/−0.37	2.14/−2.00

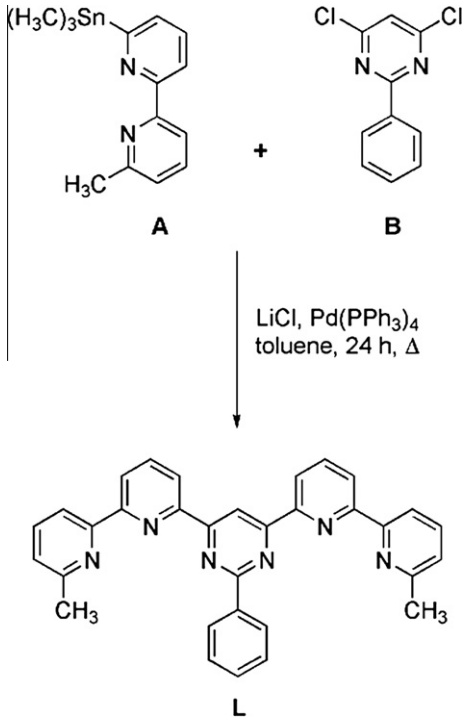

Fig. 2. Synthesis and schematic representation of bis(terpyridine) ligand **L**.

between electronic states of metal and the corresponding anions' binding capabilities. In the presence of manganese(II) perchlorates, trinuclear species $[Mn_3(\mathbf{L})_2(H_2O)_2(MeCN)_4]$ $(ClO_4)_6{\cdot}2H_2O$ **4** form with two ligand molecules **L** employed, native counterions being absent in the first coordination sphere, what is consistent with poor coordinating properties of ClO_4^-. Nevertheless when we focus on molecular packing of complex **4**, their role becomes readily discernible, since they take part in the formation of zig-zag chains via hydrogen bonding with non-coordinating water molecules present in the crystal lattice. Anions which exhibit stronger capability to coordinate namely Cl^- (**1**) or NO_3^- (**2** and **3**) prevent second **L** molecule from full saturation of metal ion in bis(tridentate) manner, which results in formation of respectively mono- $[Co(\mathbf{L})Cl_2]$ (**1**) and dinuclear $[M_2(\mathbf{L})(NO_3)_4](CH_3CN)_2$ (**2**,**3**) species. Surprisingly, halides are the salts of choice when mononuclear compounds are to be acquired, rendering ligands remaining tridentate donor pocket unaltered, in specificity and resemblance to the aforementioned $[Co(C_{21}H_{15}ClN_4)Cl_2](CH_3CN)$ [38].

Mass spectrometry was used to determine equilibrium present in solution and to further establish the nature of supramolecular architectures in terms of nuclearity. For instance: when studying $[Cu_2(\mathbf{L})(NO_3)_4](CH_3CN)_2$ (**3**) in solution, $[Cu_2(\mathbf{L})(NO_3)_3]^+$ and $[Cu(\mathbf{L})(NO_3)]^+$ are easily recognizable, more predominant being the latter one what is however obvious, at the same time demonstrating the subtle equilibrium present in solution under given conditions. This is in contrast to the solid state studies, where from magnetic susceptibility measurements it was possible to directly determine the amount of mono- and dinuclear species present (*cf.* magnetic properties). Similar species are found for $[Co_2(\mathbf{L})(NO_3)_4]$ (**2**) complexes, proving simultaneously the existence of dinuclear complexes in acetonitrile solution, which are, as magnetic properties further indicate, exclusive in the solid state. Data consistency was additionally displayed in such a manner that the highest nuclearity found for any compound never exceeded the one established by X-ray studies (which means solely 1:1 (Co:**L**) species were found for mononuclear complex $[Co\mathbf{L}Cl_2]$.

3.1. Crystal structures

Despite carrying reaction in 2:1 M ratio ($CoCl_2$:**L**) X-ray analysis of crystals acquired by slow diffusion methods revealed the following structural formula: $[Co(\mathbf{L})Cl_2]$ – **1** (Fig. 3).

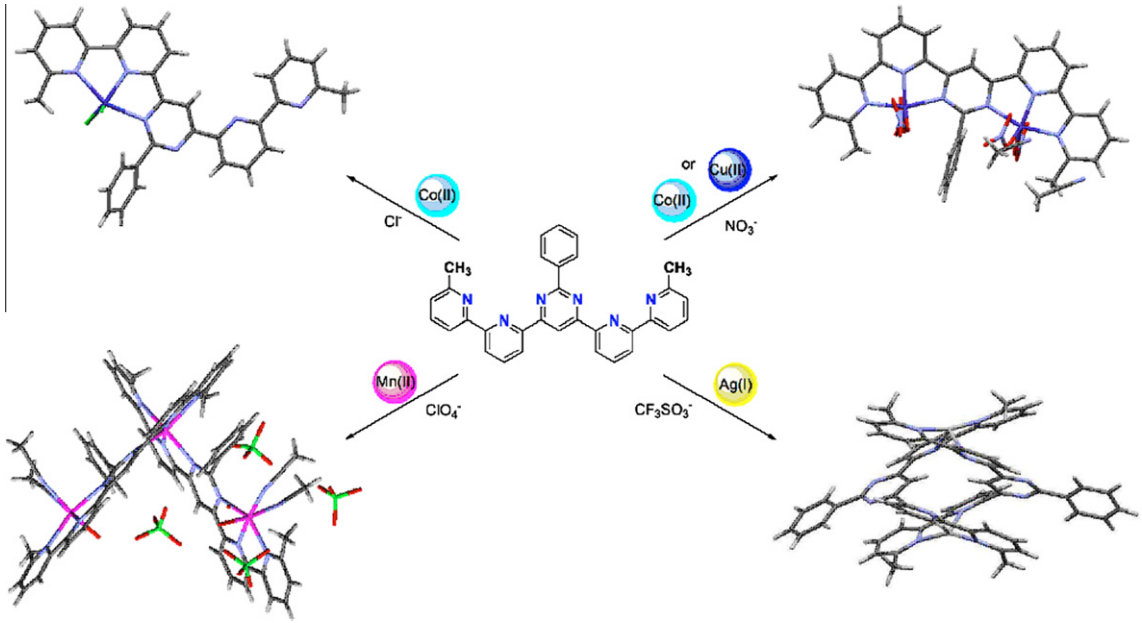

Scheme 1. Schematic representation of different supramolecular architectures formed by ligand **L**.

The Co(II) ion is five-coordinated by three ring nitrogen atoms of one half of the **L** molecule and two chlorine atoms. Interestingly in this case two halves of **L** have different disposition of nitrogen atoms: while the N atoms are all-*cis* in the coordinated part (NCCN torsion angles close to 0°), in the uncoordinated part all nitrogen atoms are *trans* with respect to each other, NCCN torsion angles are close to 180° (as expected for the uncoordinated molecule due to the H···H repulsion). The five heterocyclic rings are not far from coplanarity, the dihedral angle between the planes of terminal rings is 22.48°; the phenyl ring attached to the central ring is however significantly twisted, its plane makes the dihedral angle of 40.62(10)° to the plane of the pyrimidine ring. Geometry around the metal ion may be evaluated by means of structural index parameter τ proposed by Addison ($\tau = (\beta-\alpha/60)$, where τ ranges from 0 (undistorted square pyramidal geometry) to 1.0 (ideal trigonal bipyramidal geometry) [41]. For Co(II) ion in **1** $t = 0.34$. Surprisingly, when multiplying [Co(**L**)Cl_2] in three dimensions to form crystal lattice, one finds that the base constructive unit is one-dimensional pillar structure, its constituents arranged in a helical manner (Fig. 4) by 4_1 screw axis, what means that full 360° turn encompasses four molecules of the complex.

Overall, unit cell comprises $Z = 16$ molecules, thus four pillar-like structures may be singled out, each in relation to others by symmetry elements that is distinctive for $I4_1/a$ space group. When viewing pillars along *y* axis (Fig. 5), one may perceive two short contacts that contribute to their stability: Cl1···H–C11 (2.851(*x*) Å) and π–π (3.341(*x*) Å) stacking between central coordinating pyridine ring and the methyl substituted ring from transoidal conformation.

Furthermore, (*cf.* magnetic data) such an arrangement is responsible for the weak intermolecular antiferromagnetic interactions

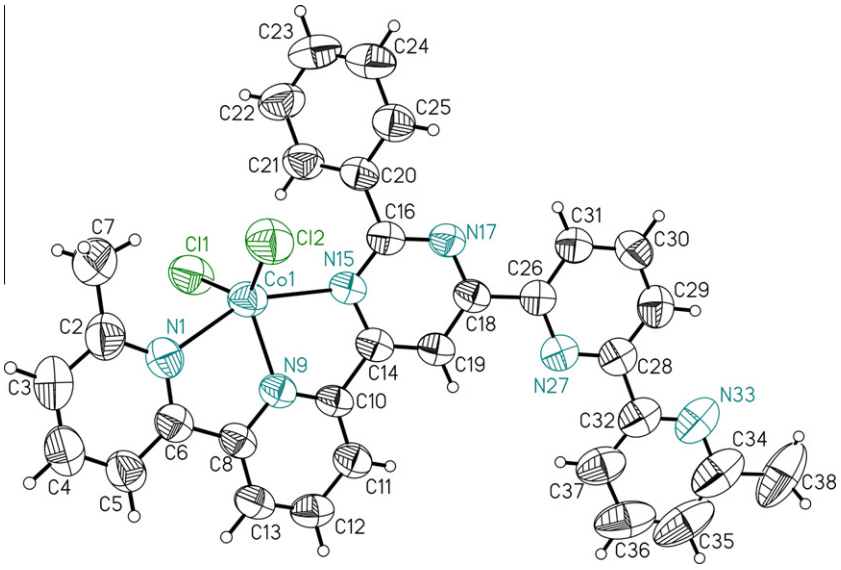

Fig. 3. Perspective view of the complex **1**; ellipsoids are drawn at 50% probability level, hydrogen atoms are shown as spheres of arbitrary radii. Relevant distances (Å): Co1–N1 2.201(3), Co1–N9 2.025(2), Co1–N15 2.268(3), Co1–Cl1 2.2923(9), Co1–Cl2 2.2579(9).

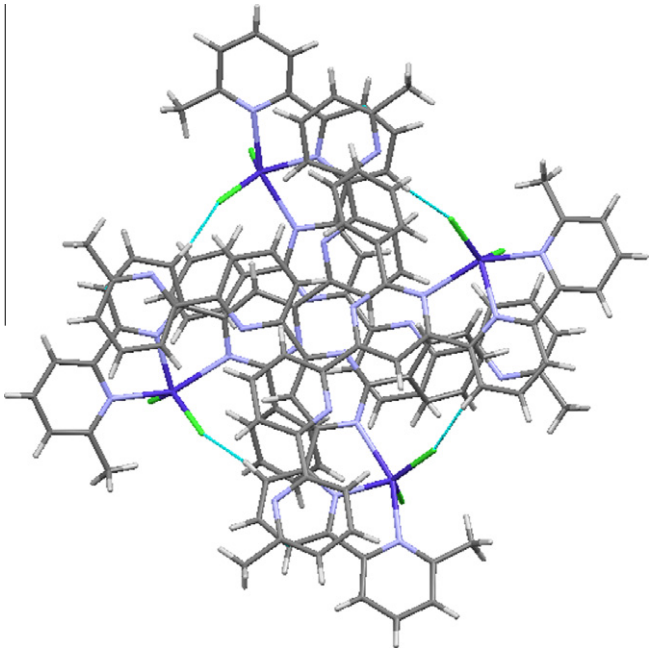

Fig. 4. 1D pillar-like constituent as seen along fourfold screw axis (*z*-direction).

between Co(II) ions in **1**. It should be however noted that non-coordinating bypyridine arm of the ligand **L** greatly contributes to the overall crystal packing of **1**, what results in large voids – Fig. 6 – with diameter of over 5 Å, where no interpretable electron density is present (*cf*. experimental section).

Its elusive role is particularly noticeable when comparing the degree of symmetry crystal structures of following compounds show: $[Co(C_{21}H_{15}ClN_4)Cl_2](CH_3CN)$ – crystal system being triclinic [38], $[Co(\mathbf{L})Cl_2]$ (**1**) – crystal system being tetragonal. Bipyridine moiety is major distinctive factor which tunes and eventually determines the outcome of self-assembly phenomena, thus it is probable that highly symmetrical crystal packing of mononuclear (**1**) system is the thermodynamically most favorable outcome of self-assembly, therefore it prevents formation of dinuclear compounds when applying halides as counterions.

In $[Co_2(\mathbf{L})(NO_3)_4](CH_3CN)_2$ (**2**) and $[Cu_2(\mathbf{L})(NO_3)_4]$ $(CH_3CN)_2$ (**3**) one molecule of **L** coordinates two cations in the baguette manner, just as it was anticipated in the experimental procedure. Since the molecules are almost identical we would discuss only the complex **2** and the data for **3** will be given in parentheses. The coordination modes of both Co(II) are very similar; the cations are five-coordinated by three N ring atoms as well and two oxygen atoms from two different nitrate anions (Figs. 7 and 8).

Due to the fact that both halves of the ligand molecule are engaged in coordination, all nitrogen atoms are in subsequent *cis* disposition, NCCN torsion angles being close to 0°. The five-ring skeleton of the ligand molecule itself is even closer to planarity than in **1**, the dihedral angle between terminal rings being only 11.3(3)° [11.2(2)°]; on the other hand, the phenyl ring is almost perpendicular to this plane, it makes the dihedral angle of 77.8(2)° [77.6(2)°] with the pyrimidine-ring plane, the latter being responsible for antiferromagnetic interactions (*cf*. magnetic data). Tau parameters equals 0.16 and 0.195 for Co1 and Co2 respectively, whereas direct distance between them is 6.264 Å [6.268 Å]. Such high degree of planarity, in relation to N-heterocyclic scaffolding, finds reflection in crystal packing which consists of sheets of dinuclear complexes alternated by voids which are occupied by acetonitrile molecules (Fig. 9).

When perchlorate ions are introduced, initial substrates self-organize into the trinuclear complex $[Mn_3(\mathbf{L})_2(H_2O)_2(MeCN)_4](ClO_4)_6{\cdot}2H_2O$ (**4**) which exhibits entirely different architecture (Fig. 10).

The structural units scaffolding involves two molecules of ligand **L** and three, unequal in binding mode, Mn(II) ions, the non-central cations' coordination spheres being further filled by two acetonitrile and one water molecules each. The complex has C_2 symmetry, the twofold axis parallel to *z* runs through the central Mn(II) ion. All metal ions are six-coordinated and the coordination polyhedra are distorted octahedra, however the ligands are in different disposition. Central manganese(II) ion Mn2 is coordinated by six nitrogen atoms from two different – but related by 2 axis – ligand molecules. The three nitrogen atoms from other halves of the ligands are involved in coordination of two other Mn(II) ions (distance between Mn2-Mn1(3) is 6.724 Å), coordination of these centers are completed by two acetonitrile and one water molecules. Two additional water molecules and six perchlorate anions occupy second coordination sphere, having direct impact on the compounds crystal packing (Fig. 11).

Two types of hydrogen bonding patterns direct trinuclear complex molecules into zig-zag chains: $O–H\cdots OH_2$ (2.734 (8) Å) resulting from interactions between water molecules – one directly bound to Mn(II) ion and the non-coordinated one; dash;$H\cdots OClO_3$ (2.795 (8) Å) bonds being the manifestation of immediate vicinity of the coordination-free water molecule and the oxygen atom of perchlorate group (Fig. 12).

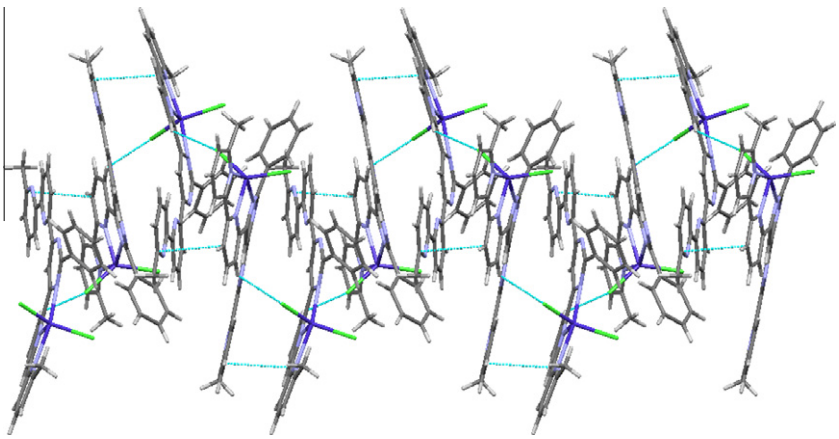

Fig. 5. 1D pillar like constituent as seen along *y* axis. Short contacts are depicted as dashed, light-blue lines. (Color online.)

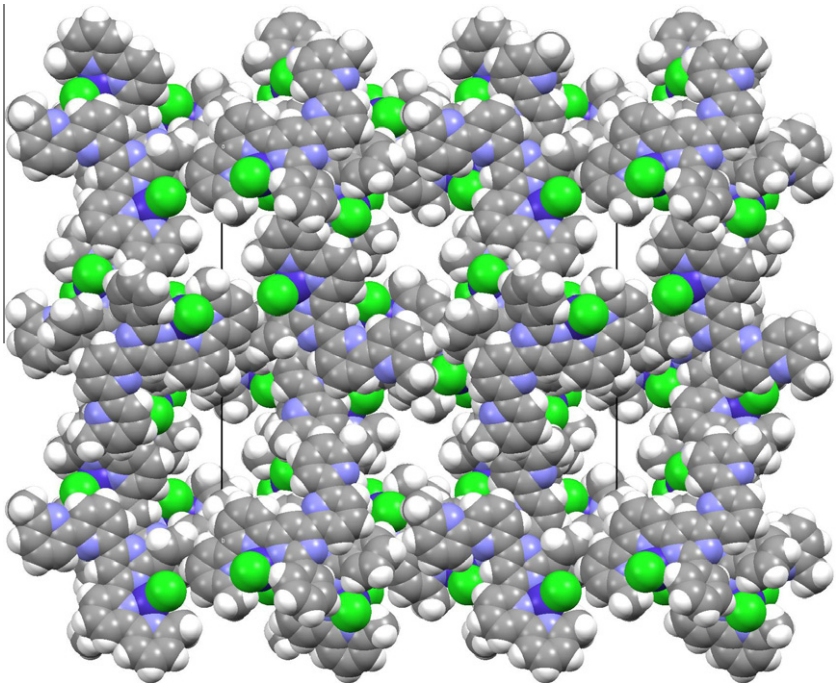

Fig. 6. The crystal packing of **1** as seen along fourfold screw axis (*z*-direction). The view shows relatively large, apparently empty voids in the crystal structure.

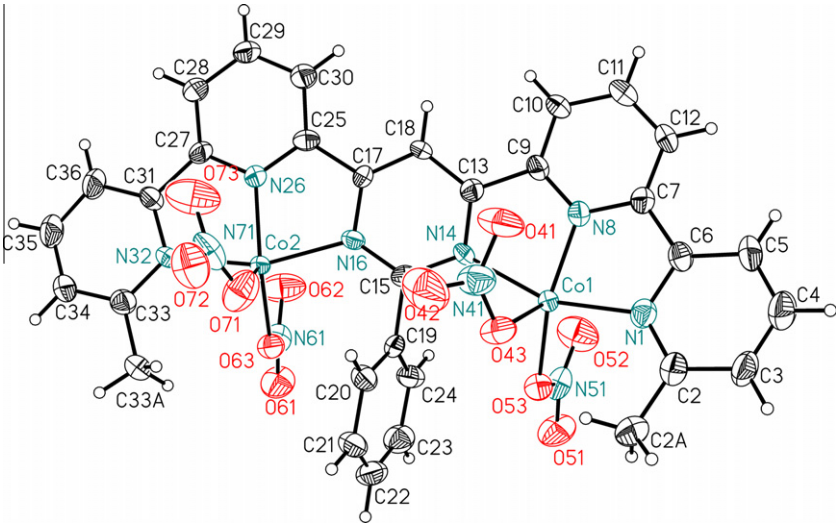

Fig. 7. ORTEP representation of the cation **2**; ellipsoids are drawn at 50% probability level, hydrogen atoms are shown as spheres of arbitrary radii. Relevant distances (Å): Co1–N1 2.038(6), Co1–N8 1.917(6), Co1–N14 2.119(5), Co1–O53 1.964(5), Co1–O43 2.137(5); Co2–N16 2.076(5), Co2–N26 1.922(5), Co2–N32 2.042(5), Co2–O63 1.962(5), Co2–O73 2.178(6).

Poor coordinative properties of ClO_4^- are responsible for exclusive synthesis of complexes that incorporate two ligand molecules **L**, being at the same time consonant with counterion dependent self-assembly process preserved in the solid state.

3.2. Magnetic properties

Magnetic properties of complexes **1**, **2**, **3** and **4** are illustrated in form of χ_m and $\chi_m T$, plotted as a function of temperature (χ_m being the molar magnetic susceptibility per one paramagnetic ion).

3.3. Cobalt complexes (*1* and *2*)

Cobalt(II), a d^7 ion in coordination compounds, can exist in a low spin doublet state or a high spin quartet state. Both spin-state configurations are known in four-, five- and six-coordinate complexes [32,33,42–49,47,50–51]. For each of these coordination numbers, systems are known where the two spin states may be thermally interconverted. The magnetic moments generally being in the range 4.7–5.2 B.M. for high spin (quartet state $^4T_{1g}$) and 1.8–2.2 B.M. for low spin (doublet state ^2E_g) complexes. The magnetic properties of molecules depend on the local geometry and the chemical links between them. In cobalt(II) complexes the decrease in the $\chi_m T$ product at low temperatures is generated by the combined effect of intramolecular antiferromagnetic interactions between the metal centers, zero-field splitting (ZFS) and the intrinsic spin–orbit coupling of the high-spin Co^{II} metal ions in octahedral surrounding. The spin–orbit coupling results in the splitting of the energy levels arising from the $^4T_{1g}$ ground term [43]. This orbital degeneracy leads to highly anisotropic interac-

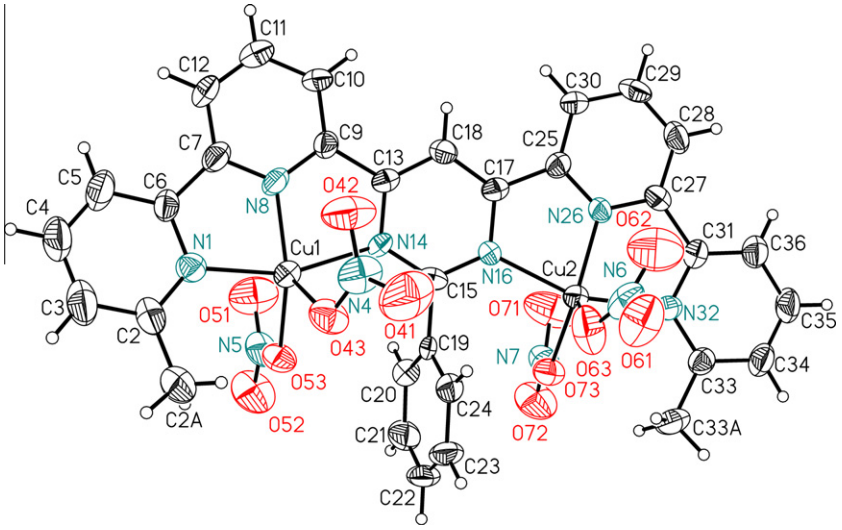

Fig. 8. Perspective view of the cation **3**; ellipsoids are drawn at 50% probability level, hydrogen atoms are shown as spheres of arbitrary radii. Relevant distances (Å): Cu1–N1 2.056(5), Cu1–N8 1.932(5), Cu1–N14 2.134(4), Cu1–O53 1.967(4), Cu1–O43 2.137(4); Cu2–N16 2.092(4), Cu2–N26 1.937(4), Cu2–N32 2.047(5), Cu2–O63 1.960(4), Cu2–O73 2.177(5).

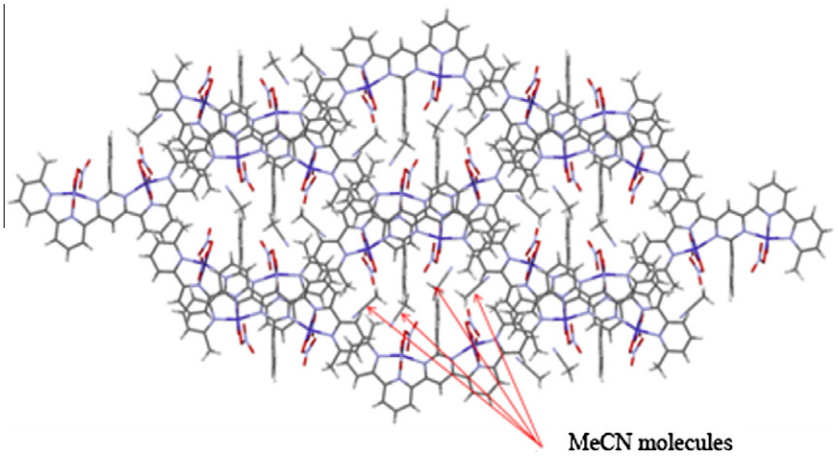

Fig. 9. Crystal packing of $[Co_2(\mathbf{L})(NO_3)_4](CH_3CN)_2$ (**2**), red arrows indicate non-coordinated acetonitrile molecules. (Color online.)

tions, the effective exchange Hamiltonian containing not only spin operators but orbital ones as well, what makes the magnetism of cobalt complexes extremely difficult to analyze [44]. In these cases the value of magnetic coupling J should be significantly reduced by taking into account the orbital reduction factor x and the spin–orbit coupling parameter λ (the Lines theory [43a]). However, if distortion from the octahedral surroundings is strong enough, then the orbital momentum is completely or partially quenched in a ligand field of a certain symmetry [45,46]. The magnetic properties of Co^{II} in the low, trigonal–bipyramidal (TBP) or square-pyramidal (SP) symmetries can be treated in a simple manner, as the ground term does not have first-order orbital angular momentum [32, 46–49,47,50,51] and a spin-only treatment is valid. The compounds $Co(terpy)X_2{\cdot}nH_20$ (terpy – terpyridine) were analysed by magnetic susceptibility measurements, in particular to study the high-spin-low-spin behavior [33,42].

Our investigations show two types of cobalt(II) bis(terpyridine) ligand complexes, mononuclear **1** and dinuclear **2** ones. The single-crystal X-ray structures of these compounds reveal a distorted square-pyramidal ligand field at each Co^{II} ion in both **1** and **2** complexes, characterized by distortion parameters $\tau = 0.34$ of **1** and 0.16, 0,195 of **2**, respectively. For that reason orbital momentum effects were neglected in magnetic interpretation. The 300 K $\chi_m T$ (T) value of **1** is 4.34 cm^3 $Kmol^{-1}$ ($\mu_{eff} = 5.89$ B.M.) and is higher than the spin – only value 3.87 B.M. for $S = 3/2$. $\chi_m T$ (T) remains nearly constant in a wide range of temperatures and smoothly decreases below 50 K to the value 1.33 cm^3 K mol^{-1} ($\mu_{eff} = 3.26$ B.M.) at 1.8 K (Fig. 13).

The slight decrease of $\chi_m T$ at low temperatures could be interpreted on the basis of zero-field splitting (ZFS) effects originated and spin–orbit coupling of Co^{II} d^7 ion and/or intermolecular antiferromagnetic interactions [32]. Taking into account magnetic anisotropy of cobalt(II) ion, the expressions of magnetic susceptibility can be derived from the spin Hamiltonian:

$$H = D[S_z^2 - 1/3S(S+1)] + g_{\|}\beta H_z S_z + g_{\perp}\beta(H_x S_x + H_y S_y) \quad (3)$$

where DS_z^2 represents the splitting into two Kramers doublets in the absence of a magnetic field, ($|D|$ being the energy gap between the Kramers doublets $|\pm 3/2>$ and $|\pm 1/2>$).

The $\chi_m T$ data were well fit by the Curie–Weiss expression [32,51]:

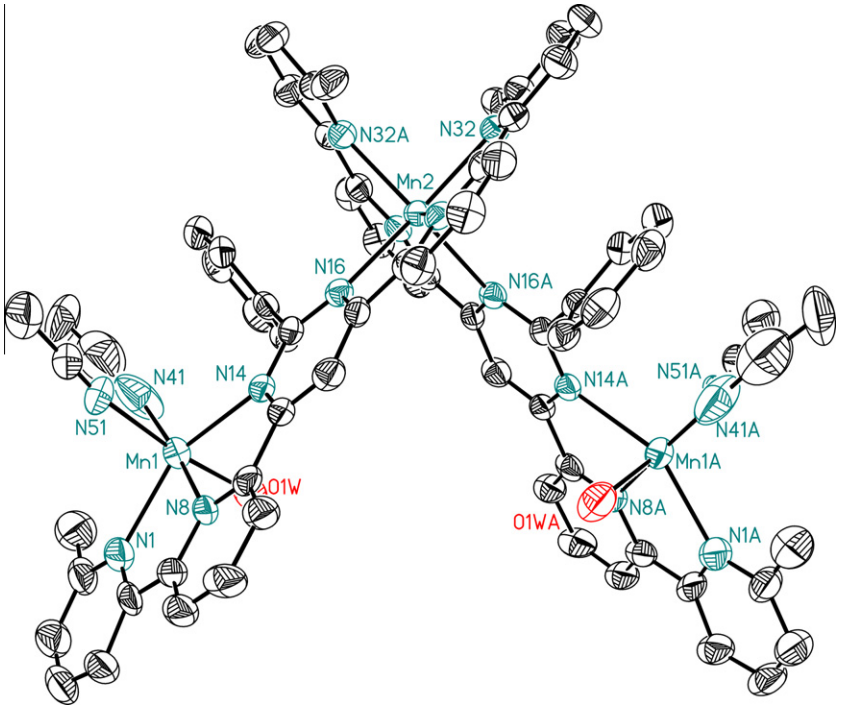

Fig. 10. Perspective view of the cation **4**; ellipsoids are drawn at 33% probability level, hydrogen atoms are omitted for clarity. Relevant distances (Å): Mn1–N1 2.298(6), Mn1–N8 2.196(6), Mn1–N14 2.360(6), Mn1–N41 2.112(9), Mn1–N51 2.263(8), Mn1–O1W 2.155(6), Mn2–N16 2.407(5), Mn2–N26 2.196(5), Mn2–N32 2.261(5). The letter A denotes the symmetry code $3/2 - x$, $1/2 - y$,z.

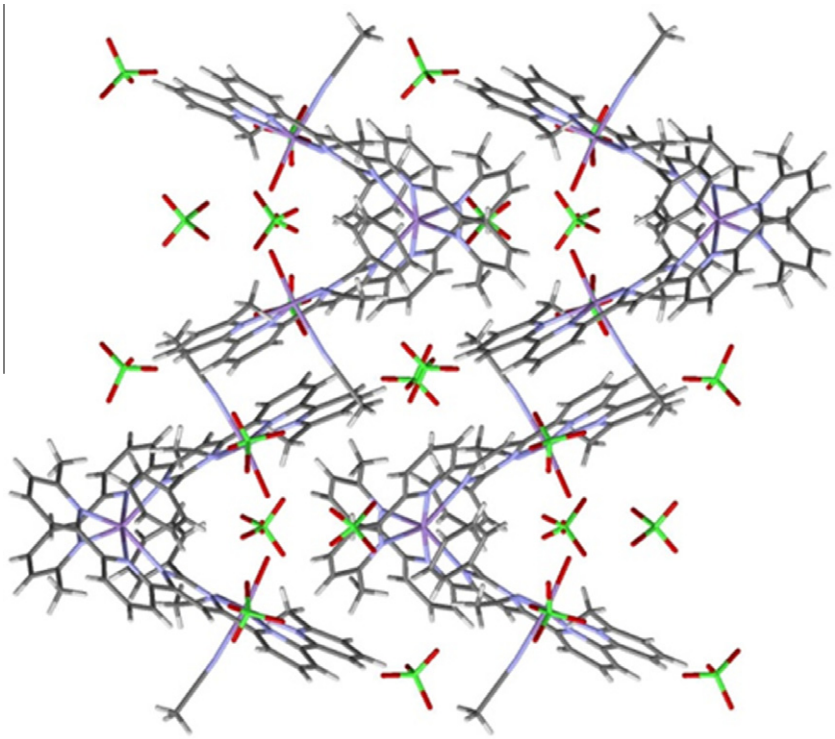

Fig. 11. Zig-zag chains of $[Mn_3(\mathbf{L})_2(H_2O)_2(MeCN)_4]$ $(ClO_4)_6{\cdot}2H_2O$ (**4**) as seen along y axis.

$$\chi = \frac{1}{3}\frac{N\beta^2 g_{\parallel}^2 S(S+1)}{k(T-\theta)}\left(\frac{1+9e^{-2D/kT}}{4+(1+e^{-2D/kT})}\right)+\frac{2}{3} \times \frac{N\beta^2 g_{\perp}^2 S(S+1)}{k(T-\theta)}\left(\frac{1+\frac{3T}{4D}(1-e^{-2D/KT})}{1+e^{-2D/kT}}\right) \quad (4)$$

where $g_{\parallel}$ and $g_{\perp}$ are the spectroscopic splitting factors, N-the Avogadro number, β the Bohr magneton, k the Boltzman constant and T is the absolute temperature.

Least-squares fitting of the data of **1** leads to $D = 13\ cm^{-1}$, $g_{\perp} = 2.08$, $g_{\parallel} = 2.45$ $\theta = -0.7\ cm^{-1}$ $R = 2.73 \times 10^{-5}$.

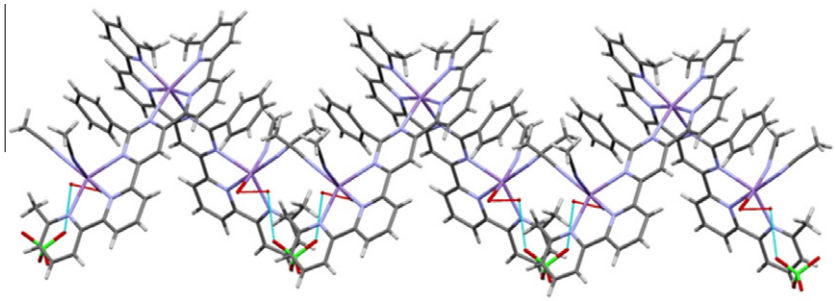

Fig. 12. Crystal packing of $[Mn_3(\mathbf{L})_2(H_2O)_2(MeCN)_4](ClO_4)_6{\cdot}2H_2O$ (**4**) directed by hydrogen bonds; O–H···OH_2 and O–H···$OClO_3$ contacts are represented by red and light-blue lines respectively. (Color online.)

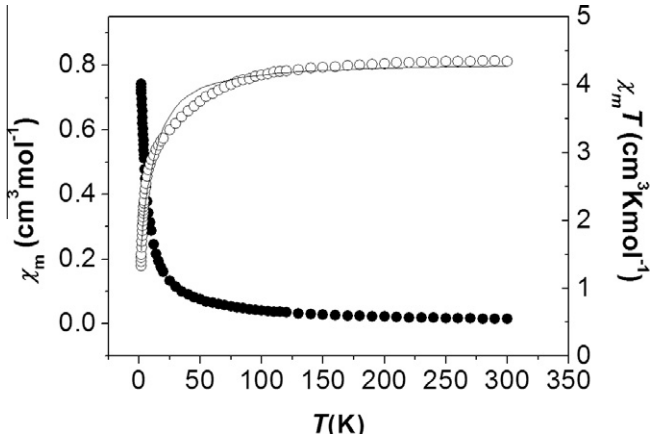

Fig. 13. Temperature dependences of experimental χ_m and $\chi_m T$ vs. T for complex **1**. The solid lines are the calculated curves, with parameters presented in the text.

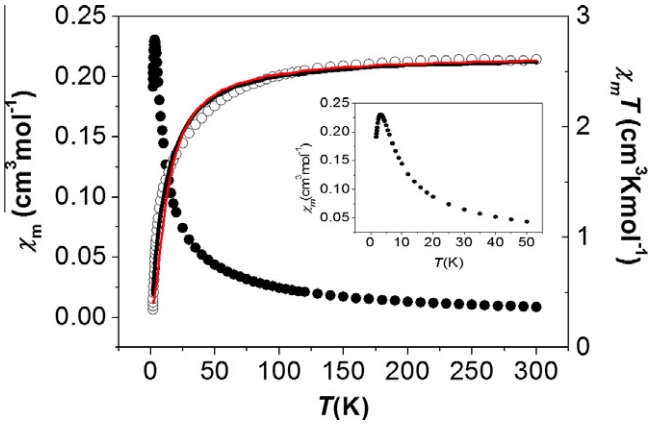

Fig. 14. Temperature dependences of experimental χ_m and $\chi_m T$ vs. T for complex **2**. The solid lines are the calculated curves, with parameters presented in the text. The inset shows the χ_m curve in the low temperature range.

The negative $\theta = -0.7\ cm^{-1}$value informs about weak intermolecular antiferromagnetic interactions as a results of short intermolecular contacts along y axis of 1D pillar-like constituent of **1** (Cl1···H–C11 and π–π stacking).

In complex **2** maximum of magnetic susceptibility was observed at 4 K (Fig. 14), which indicated antiferromagnetic coupling within the dinuclear species.

The same model was used for dinuclear cobalt complex **2**, comparable $D = 13\ cm^{-1}$, $g_{\perp} = 2.08$, $g_{||} = 2.55$ ($g_{av} = 2.40$) fitting parameters were obtained and negative Weiss constant $\theta = -4.2\ cm^{-1}$ ($R = 1.07 \times 10^{-4}$). The magnetic data of **2** were also approximately modeled by using an isotropic Heisenberg spin Hamiltonian: $H = -4J(S_{Co1}S_{Co2})$, where J is the exchange interactions within the [Co_2] complex [46,47,51], $D = 13\ cm^{-1}$ was used as constant and the van Vleck expression of the magnetic susceptibility as:

$$\chi^T = \frac{N\beta^2 g^2}{k}\frac{2e^{2J/kT} + 10e^{6J/kT} + 28e^{12J/kT}}{1 + 3e^{2J/kT} + 5e^{6J/kT} + 7e^{12J/kT}} \quad (5)$$

Good approximation (*cf.* red solid line Fig. 14) was obtained with the parameters: $g = 2.33$, $J = -1.70\ cm^{-1}$, $R = 1.80 \times 10^{-4}$.

3.4. Copper complex

In the case of copper **3** complex, the existence of dinuclear as well as mononuclear form is observed in temperature dependence of magnetic susceptibility (Fig. 15).

The magnetic susceptibility reaches a maximum at about 40 K, then decreases with temperature lowering to a minimum value at 15 K. Further temperature decreasing results in an increase of χ_m suggesting the presence of monomeric form in this sample. Susceptibility maximum indicates an antiferromagnetic exchange interactions between two copper(II) centers, defined by spin Hamiltonian $H = -J\Sigma S_1 S_2$ where J is the coupling constant. The compound obeys Curie–Weiss law above 100 K, with Curie $C = 0.431\ cm^3\ K\ mol^{-1}$ and Weiss $\theta = -17$ K constants. Negative value of Weiss constant confirms antiferromagnetic interactions between copper(II) ions.

The magnetic data of the complex **3** were fitted using modified Bleaney–Bower's equation [32]:

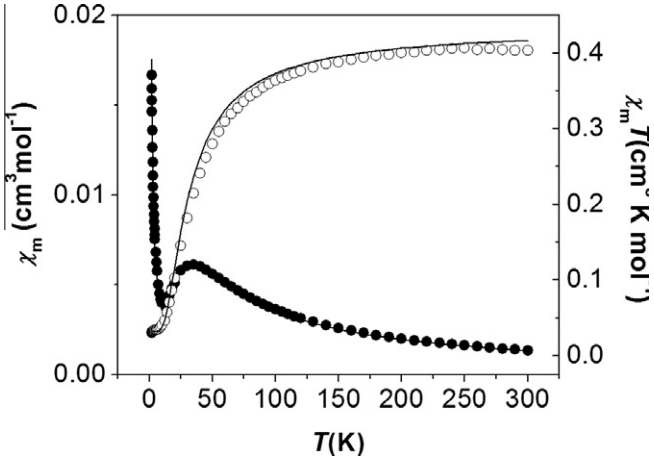

Fig. 15. Temperature dependences of experimental χ_m and $\chi_m T$ vs. T for complex **3**. The solid lines are the calculated curves, with parameters presented in the text.

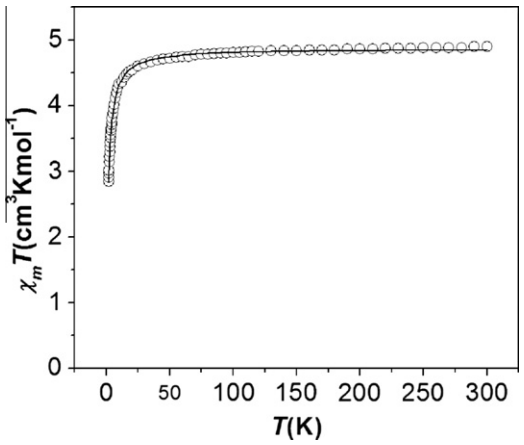

Fig. 16. Temperature dependence of experimental $\chi_m T$ vs. T for complex **4**. The solid lines are the calculated curves, with parameters presented in the text.

$$\chi_m = \left\{\frac{Ng_{\mathrm{dim}}^2\beta^2}{3kT}\left[1+\frac{1}{3}\left(e^{-j/kT}\right)\right]^{-1}\right\}(1-x)+\left(\frac{Ng_{\mathrm{mon}}^2\beta^2}{4kT}\right)x \qquad (6)$$

where x is the mole fraction of the monomeric form, and g_{mon} and g_{dim} are spectroscopic splitting factors of the monomer and dimer forms, respectively, the other symbols have the usual meaning. Magnetic parameters: $g_{\mathrm{dim}} = 2.12$, $g_{\mathrm{mon}} = 2.12$, $2J = -40\ \mathrm{cm}^{-1}$ and monomeric form at level 7.5% were obtained, $R = 3.5 \times 10^{-4}$.

Magnetic methods are very sensitive to identify monomeric impurity existing very often in dimeric copper complexes and useful to characterize amount of noncoupled species in the sample [32]. The resulted singlet–triplet energy gap $2J$ is in good agreement with the temperature of magnetic susceptibility maximum. The temperature T_{max} is related to $2J$ according to: $|2J|/kT_{\mathrm{max}} = 1.599$ [32] and observed values follow this relation.

3.5. Manganese complex

Magnetic data of six coordinated manganese(II) complex **4** were calculated per tri-Mn^{II} clusters according to the crystal structure. High spin $S = 5/2$ with $\mu_{\mathrm{eff}} = 5.98$ B.M. ($\chi_m T = 4.46\ \mathrm{cm}^3\ \mathrm{K\ mol}^{-1}$) is observed at 300 K. The $\chi_m T$ is practically constant in the whole experimental temperature range (Fig. 16). Only a slight decrease, observed at the lowest temperatures, below 10 K may suggest weak antiferromagnetic interactions between Mn^{II} ions. The magnetic exchange interactions within the tri-Mn^{II} clusters are mediated through pyrimidine bridge and there exists only one exchange constant J, thus the isotropic spin Hamiltonian is described as follows: $H = 2J(S_1S_2 + S_2S_3)$, neglecting interactions between S_1S_3.

The equation of molar susceptibility of trinuclear cluster [52]:

$$\chi_{tri} = \frac{Ng^2\beta^2}{4kT} \times \frac{1+20e^{3J/kT}+105e^{8J/kT}+210e^{15J/kT}+330e^{24J/kT}+429e^{35J/kT}+455e^{48J/kT}+340e^{63J/kT}}{1+4e^{3J/kT}+9e^{8J/kT}+10e^{15J/kT}+10e^{24J/kT}+9e^{35J/kT}+7e^{48J/kT}+4e^{63J/kT}} \qquad (7)$$

and molecular field model of magnetic interactions were used:

$$\chi_m^{corr} = \frac{\chi_{tri}}{1-\frac{2zJ'}{N\beta^2g^2}\cdot\chi_{tri}} \qquad (8)$$

where N – the Avogadro's number, g – the spectroscopic splitting factor, β – the Bohr magneton, k – the Boltzmann constant and T is the absolute temperature, J – intramolecular exchange within tri-Mn^{II} cluster, zJ' – intermolecular magnetic exchange parameter, z is number of interacting molecules. The best fit parameters: $g = 2.0$, $J = -0.10\ \mathrm{cm}^{-1}$, $zJ' = -0.02\ \mathrm{cm}^{-1}$ confirm very weak antiferromagnetic interactions between Mn^{II} ions.

Similar very weak antiferromagnetic interactions between Mn^{II} ions through 1,3-diazine (pyrimidine) and 1,4-diazine (pyrazine) were observed by Ishida et al. [47] and by us, recently [53,56]. In comparison of the magnitude of magnetic interactions between Co^{II}, Cu^{II} and Mn^{II} compounds (**2**, **3** and **4**) with other pyrimidine and pyrazine bridged systems, the net antiferromagnetic interactions, defined by n^2J instead of J, is more appropriate, were n being the number of magnetic orbitals (the number of unpaired electrons of the metal center) [32,54,55].

In the Table 2 we collected exchange parameters, expressed as J, n^2J, as well as $2J/k_B$.

Collected experimental data present weak antiferromagnetic interactions and suggest that the metal(II) sites communicate through the planar, π-delocalized diazine rings in the coupled subunits. Comparable values of magnetic coupling parameters were obtained for complexes with the same metal ions. Analyzed by us complexes **2**, **3** and **4** confirm that he highest magnitude of interactions was observed for Cu^{II} coupled dimers, however, similar metal to metal separation across the bridging diazine rings (from 6.495 to 6.725 Å) for all presented complexes were observed. Because of planarity of diazine ring the $d_{x^2-y^2}$ type magnetic orbital of copper(II) ion (in a square pyramidal geometry in **3** and in [57]) is mainly located in the basal xy plane. The significant σ-overlap between two magnetic orbitals through bridging ring would account for the antiferromagnetic coupling observed in this family.

Table 2
Exchange parameters for pyrimidine and pyrazine bridged compounds.

M^{II}	J(cm^{-1}) [a]	n^2J	$2J/k_B$ (K)[b]	Model of interactions (bridge)	Ref.
Co **2**	−1.7	−15.3	−2.44	dimer (pyrimidine)	this work
Cu **3**	−40	−40	−57.6	dimer + monomer (pyrimidine)	this work
Mn **4**	−0.1	−2.5	−0.28	trimer (pyrimidine)	this work
Mn	−0.22	−5.50	−0.32[c]	dimer (pyrazine)	[56]
Mn	−0.29	−7.25	−0.42[c]	tetramer (pyrazine)	[56]
Mn	−0.28[c]	−7.0	−0.40	dimer (pyrazinedicarboxylate)	[47]
Mn	−0.26[c]	−6.5	−0.38	dimer (pyrimidinedicarboxylate)	[47]
Co	−2.15	−19.4	−3.1	dimer (pyrimidinedicarboxylate)	[47]
Cu	−32[c]	−32[c]	−46	dimer (pyrimidinedicarboxylate)	[47]
Cu	−40.9	−40.9[c]	−58.8[c]	dimer (pyrazine)	[57]
Cu	−17.2 to −21.2[c]	−17.2 to −21.2[c]	−24.7 to −30.5	dimer (2-pyridylpyrazine)	[58]

[a] J = singlet–triplet energy gap.
[b] $2J$ = singlet–triplet energy gap.
[c] Calculated from the value presented in the literature.

4. Conclusions

The ability of new bis(terpyridine) ligand **L** to stabilize mono- and polynuclear metal species enables the facile synthesis of novel supramolecular architectures. X-ray crystal structures have revealed that depending on the counterions applied, one may obtain mono- $[Co(\mathbf{L})Cl_2]$ (**1**), di- $[M_2(\mathbf{L})(NO_3)_4](CH_3CN)_2$ (**2** or **3**) or trinuclear $[Mn_3(\mathbf{L})_2(H_2O)_2(MeCN)_4]$ $(ClO_4)_6{\cdot}2H_2O$ (**4**) species, self-assembly being as well determined by the appropriate choice of the metal ion. In particular it is revealed upon insight into complexes' crystal structures: non-coordinating terpyridine subunit of mononuclear **1** accounts for organization into one-dimensional pillar-like helical constituents; strongly coordinating nitrate anions of isostructural **2** and **3** renders solely the formation of irregular molecular sheets possible; poorly coordinating ClO_4^- species, together with water molecules are responsible for the existence of zig-zag shaped chains present in **4**. Metal ions have been found to exhibit both high-spin multiplicity and antiferromagnetic coupling, as indicated by magnetic susceptibility measurements. Our contribution provides not only an avenue for preparing new potential functional materials [59] but is also an essential input of work which considers taming the complexity. Further studies will involve exploitation of potential applicative interest of newly synthesized compounds such as for instance determination of porosity for **1** which may act as potential 'molecular sieve' (*cf*. its relatively low density, Table 1) [60].

Acknowledgements

We would like to express our deep gratitude to Prof. Jean-Marie Lehn for the opportunity to carry out a part of these studies in his laboratory and for his precious advice. This research was carried out as a part of the National Science Center project (Grant No. 2011/03/B/ST5/01036).

Appendix A

Crystallographic data (excluding structure factors) for the structural analysis has been deposited with the Cambridge Crystallographic Data Centre, Nos. CCDC – 852516 (**1**), CCDC - 852517 (**2**), CCDC – 853865 (**3**) and CCDC – 852518 (**4**). Copies of this information may be obtained free of charge from: The Director, CCDC, 12 Union Road, Cambridge, CB2 1EZ, UK. Fax:+44 1223 336 033, e-mail:deposit@ccdc.cam.ac.uk, or www: www.ccdc.cam.ac.uk.

References

[1] J.-M. Lehn, Supramolecular Chemistry: Concepts and Perspectives, Wiley-VCH, Weinheim, 1995.
[2] A. Wild, A. Winter, F. Schlütter, U.S. Schubert, Chem. Soc. Rev. 40 (2011) 1459.
[3] M. Ruben, J. Rojo, F.J. Romero-Salguero, L.H. Uppadine, J.-M. Lehn, Angew. Chem., Int. Ed. 43 (2004) 3644.
[4] J.R. Price, N.G. White, A. Perez-Velasco, G.B. Jameson, C.A. Hunter, S. Brooker, Inorg. Chem. 47 (2008) 10729.
[5] L.K. Thompson, Coord. Chem. Rev. 233–234 (2002) 193.
[6] L.N. Dave, K.V. Shuavev, L.K. Thompson, Inorg. Chem. 48 (2009) 3323.
[7] E.C. Constable, S. Decurtins, C.E. Housecroft, T.D. Keene, C.G. Palivan, J.R. Price, J.A. Zampese, Dalton Trans. 39 (2010) 2337.
[8] A.R.K. Glasson, L.F. Lindoy, G.V. Meehan, Coord. Chem. Rev. 252 (2008) 940.
[9] A.R. Stefankiewicz, M. Wałęsa, P. Jankowski, A. Ciesielski, V. Patroniak, M. Kubicki, Z. Hnatejko, J.M. Harrowfield, J.-M. Lehn, Eur. J. Inorg. Chem. (2008) 2910.
[10] Q.-F. Sun, J. Iwasa, D. Ogawa, Y. Ishido, S. Sato, T. Ozeki, Y. Sei, K. Yamaguchi, M. Fujita, Science 328 (2011) 1144.
[11] T.B. Gasa, C. Valente, J.F. Stoddart, Chem. Soc. Rev. 40 (2011) 57.
[12] C. Oelschlaeger, P. Suwita, N. Willenbacher, Langmuir 26 (2010) 7045.
[13] D. Li, J. Song, P. Yin, S. Simotwo, A.J. Bassler, Y.Y. Aung, J.E. Roberts, K.I. Hardcastle, C.L. Hill, T. Liu, J. Am. Chem. Soc. 133 (2011) 14010.
[14] M. Kaller, C. Deck, A. Meister, G. Hause, A. Baro, S. Laschat, Chem. Eur. J. 16 (2010) 6326.
[15] M. Distaso, R.N.K. Taylor, N. Taccardi, P. Wasserscheid, W. Peukert, Chem. Eur. J. 17 (2011) 2923.
[16] C. Desmarets, I. Azcarate, G. Gontard, H. Amouri, Eur. J. Inorg. Chem. (2011) 4558.
[17] A. Winter, S. Hoeppener, G.R. Newkome, U.S. Schubert, Adv. Mater. 23 (2011) 3484.
[18] G.R. Winter, U.S. Newkome, ChemCatChem 3 (2011) 1384.
[19] S. Roy, S. Saha, R. Majumdar, R.R. Dighe, A.R. Chakravarty, Polyhedron 29 (2010) 3251.
[20] D. Zabel, A. Schubert, G. Wolmershäuser, Eur. J. Inorg. Chem. 23 (2008) 3648.
[21] V. Artero, M. Chavarot-Kerlidou, M. Fontecave, Angew. Chem., Int. Ed. 50 (2011) 7238.
[22] J. Boonmak, M. Nakano, N. Chaichit, C. Pakawatchai, S. Youngme, Inorg. Chem. 5 (2011) 7324.
[23] D.G. Nocera, B.M. Bartlett, D. Grohol, D. Papoutsakis, M.P. Shores, Chem. Eur. J. 10 (2004) 3850.
[24] W. Li, P.T. Barton, R.P. Burwood, A.K. Cheetham, Dalton Trans. 40 (2011) 7147.
[25] M.-H. Zeng, W.-X. Zhang, X.-Z. Sun, X.-M. Chen, Angew. Chem., Int. Ed. 44 (2005) 3079.
[26] E.-C. Yang, Z.-Y. Liu, Y.-L. Li, J.-Y. Wang, X.-J. Zhao, Dalton Trans. 40 (2011) 8513.
[27] V. Patroniak, M. Kubicki, A.R. Stefankiewicz, A.M. Grochowska, Tetrahedron 61 (2005) 5475.
[28] K. Burdeska, H. Fuhrer, G. Kabas, A.E. Siegriest, Helv. Chim. Acta 64 (1981) 113.
[29] Agilent Technologies, CrysAlis PRO (Version 1.171.33.36d). Agilent Technologies Ltd., 2011.
[30] A. Altomare, G. Cascarano, C. Giacovazzo, A. Gualardi, J. Appl. Crystallogr. 26 (1993) 343.
[31] G.M. Sheldrick, Acta Crystallogr., Sect. A 64 (2008) 112.
[32] O. Kahn, Molecular Magnetism, Willey-VCH, 1993.
[33] H.A. Goodwin, Top. Curr. Chem. 234 (2004) 23.
[34] V. Patroniak, A.R. Stefankiewicz, J.-M. Lehn, M. Kubicki, Eur. J. Inorg. Chem. (2005) 4168.
[35] V. Patroniak, P.N.W. Baxter, J.-M. Lehn, M. Kubicki, M. Nissinen, K. Rissanen, Eur. J. Inorg. Chem. (2003) 4001.
[36] V. Patroniak, P.N.W. Baxter, J.-M. Lehn, Z. Hnatejko, M. Kubicki, Eur. J. Inorg. Chem. (2004) 2379.
[37] M. Ruben, E. Breuning, M. Barboiu, J.-P. Gisselbrecht, J.-M. Lehn, Chem. Eur. J. 9 (2003) 291.
[38] A. Ciesielski, A. Gorczyński, P. Jankowski, M. Kubicki, V. Patroniak, J. Mol. Struct. 973 (2010) 130.
[39] I. Iwakura, T. Ikeno, T. Yamada, Angew. Chem., Int. Ed. 44 (2005) 2524.
[40] M. Wałęsa-Chorab, V. Patroniak, M. Kubicki, G. Kądziołka, J. Przepiórski, B. Michalkiewicz, J. Catal. 291 (2012) 1.
[41] A.W. Addison, T.N. Rao, J. Reedijk, J. VanRijn, G.C. Verschoor, J. Chem. Soc., Dalton Trans. (1984) 1349.
[42] S. Kremer, W. Henke, D. Reinen, Inorg. Chem. 21 (1982) 3013.
[43] a M.E. Lines, J. Chem. Phys. 55 (1971) 2977;
b F. Lloret, M. Julve, J. Cano, R. Ruiz-Garcia, E. Pardo, Inorg. Chim. Acta 361 (2008) 3432;
c G. De Munno, T. Poerio, M. Julve, F. Lloret, G. Viau, New J. Chem. (1998) 299.
[44] J. Olguín, M. Kalisz, R. Clérac, S. Brooker, Inorg. Chem. 51 (2012) 5058.
[45] S.M. Ostrovsky, K. Falk, J. Pelikan, D.A. Brown, Z. Tomkowicz, W. Haase, Inorg. Chem. 45 (2006) 688.
[46] M. Sarkaz, R. Clérac, C. Mathonière, N.G.R. Hearns, V. Bertolasi, D. Ray, Eur. J. Chem. (2009) 4675.
[47] T. Ishida, T. Kawakami, S. Mitsubori, T. Nogami, K. Yamaguchi, H. Iwamura, J. Chem. Soc., Dalton Trans. (2002) 3177.
[48] M.-H. Zeng, S. Gao, X.-M. Chen, Inorg. Chem. Commun. 7 (2004) 864.
[49] J.S. Maass, M. Zeller, T.M. Breault, B.M. Bartlett, H. Sakiyama, R.L. Luck, Inorg. Chem. 51 (2012) 4903.
[50] S.M. Ostrovsky, R. Werner, D.A. Brown, W. Haase, Chem. Phys. Lett. 353 (2002) 290.
[51] E. Shurdha, C.E. Moore, A.L. Rheingold, J.S. Miller, Inorg. Chem. 50 (2011) 10546.
[52] L. Chen, D. Shi, J. Zhao, Y. Wang, P. Ma, J. Wang, J. Niu, Cryst. Growth Des. 11 (2011) 1913.
[53] M. Wałęsa-Chorab, A.R. Stefankiewicz, D. Ciesielski, Z. Hnatejko, M. Kubicki, J. Kłak, M. Korabik, V. Patroniak, Polyhedron 30 (2011) 730.
[54] G. Beobide, O. Castillo, A. Luque, U. García-Couceiro, J.P. García-Terán, P. Román, Inorg. Chem. 45 (2006) 5367.
[55] L. Rodrigez, E. Labisbal, A. Sousa-Pedrares, J.A. Garcia-Vázquez, J. Romero, M.L. Duran, J.A. Real, A. Sousa, Inorg. Chem. 45 (2006) 7903.
[56] M. Wałęsa-Chorab, M. Kubicki, M. Korabik, Violetta Patroniak, submitted.
[57] J. Carranza, J. Sletten, C. Brennan, F. Lloret, J. Cano, Dalton Trans. (2004) 3997.
[58] E. Burkholder, V. Golub, Ch.J. O'Connor, J. Zubieta, Inorg. Chem. 42 (2003) 6729.
[59] M.D. Allendorf, A. Schwartzberg, V. Stavila, A.A. Talin, Chem. Eur. J. 17 (2011) 11372.
[60] S.D. Burd, S. Ma, J.A. Perman, B.J. Sikora, R.Q. Snurr, P.K. Thallapally, J. Tian, L. Wojtas, M.J. Zaworotko, J. Am. Chem. Soc. 134 (2012) 3663.